

Unsupervised Domain Adaptation for 3D Keypoint Prediction from a Single Depth Scan

Xingyi Zhou

The University of Texas at Austin

zhouxy@cs.utexas.edu

Arjun Karapur

The University of Texas at Austin

akarpur@cs.utexas.edu

Chuang Gan

Tsinghua University

ganchuang1990@gmail.com

Linjie Luo

Snap, Inc.

linjie.luo@snap.com

Qixing Huang

The University of Texas at Austin

huangqx@cs.utexas.edu

Abstract

In this paper, we introduce a novel unsupervised domain adaptation technique for the task of 3D keypoint prediction from a single depth scan/image. Our key idea is to utilize the fact that predictions from different views of the same or similar objects should be consistent with each other. Such view consistency provides effective regularization for keypoint prediction on unlabeled instances. In addition, we introduce a geometric alignment term to regularize predictions in the target domain. The resulting loss function can be effectively optimized via alternating minimization. We demonstrate the effectiveness of our approach on real datasets and present experimental results showing that our approach is superior to state-of-the-art general-purpose domain adaptation techniques.

1. Introduction

A new era has arrived with the proliferation of depth-equipped sensors in all kinds of form factors, ranging from wearables and mobile phones to on-vehicle scanners. This ever-increasing amount of depth scans is a valuable resource that remains largely untapped, however, due to a lack of techniques capable of efficiently processing, representing, and understanding them.

3D keypoints, which can be inferred from depth scans, are a compact yet semantically rich representation of 3D objects that have proven effective for many tasks, including reconstruction [11], object segmentation and recognition [17], as well as pose estimation [32]. Despite the wide availability of depth scans of various categories of objects [4], there is a lack of 3D keypoint annotations for them, which are necessary to train reliable keypoint predictors. This deficit is due to the fact that depth scans are inherently par-

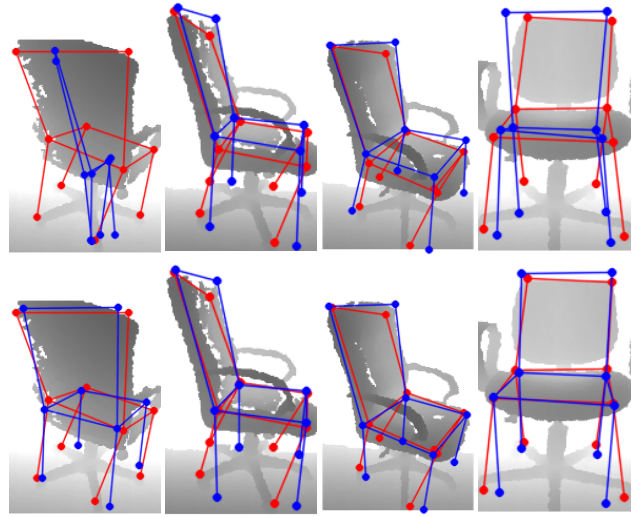


Figure 1: Our proposed unsupervised domain adaptation approach improves 3D keypoint prediction results from single depth scans of the Redwood dataset [4]. **(Top)** without domain adaptation, the pre-trained keypoint predictor from simulated examples failed to predict accurate 3D keypoints (blue). **(Bottom)** 3D keypoint predictions (blue) after domain adaptation are significantly improved. Note that the ground-truth keypoints are shown in red for comparison.

tial views of the underlying objects, making it difficult to annotate the object parts occluded from view. One could automate the annotation process by leveraging the “fused” models created using the depth scans, but most depth-fusion methods are susceptible to scanning noise and cascading errors when depth scans are captured at scale [4].

In this paper, our goal is to predict 3D keypoints of an underlying object from a single raw depth scan. To train a reliable 3D keypoint predictor, we generate a large dataset of simulated depth scans using large-scale 3D model repos-

itories such as ShapeNet [3] and ModelNet [37]. The 3D keypoint annotations on the 3D models from these repositories can naturally carry over to the simulated depth scans for effective supervised training. A large gap exists, however, between the simulated and real depth scan domains. Particularly, 3D models from repositories are generally designed with interactive tools, inevitably resulting in inaccurate geometries with varying scales. Further, the real depth scans contain noticeable measurement noise and background objects, and the class distributions of 3D models from the repositories and those from real depth scans may be different.

To close the gap between the source domain of simulated depth scans and the target domain of real depth scans, we introduce a novel approach for unsupervised domain adaptation of 3D keypoint prediction. Our approach is motivated by the special spatial properties of the 3D keypoints and the relationship between the keypoint distributions of the source and target domains.

First, keypoint predictions from different views of the same 3D model should be consistent with each other up to a pose transformation. This allows us to formulate a *view-consistency* regularization to propagate a good prediction, e.g. from a well-posed view where the prediction is more accurately adapted, to a challenging view with less accurate adaptation. To this end, we introduce a latent keypoint configuration to fuse the keypoint predictions from different views of the same object. Additionally, we introduce a pose-invariant metric to compare the keypoint predictions, which allows us to use depth scans without camera pose calibration for training.

Second, despite the distinctive differences between the source and target domains, their 3D keypoint distributions are highly correlated. However, naively aligning the 3D keypoint distributions between the two domains is sub-optimal since the occurrences of the same type of objects differ. We propose a *geometric alignment* regularization that is insensitive to varying densities of the objects in order to align the keypoint distributions of the two domains. We make use of the target domain’s latent keypoint configurations from view consistency regularization to compute the geometric alignment with the source domain. Note that since possible keypoint configurations lie on a manifold with much lower dimension over the ambient space, the geometric alignment can provide effective regularization.

Our final formulation combines a standard supervised loss on the source domain with the two unsupervised regularization losses on view-consistency and geometric alignment. Our formulation can be easily optimized via alternating minimization and admits a simple strategy for variable initialization.

We evaluate the proposed approach on unsupervised domain adaptation from ModelNet [37] to rendered depth

scans from the synthesized ShapeNet [3] 3D model dataset, and to real depth scans from the Redwood Object Scans [4] and 3DCNN Depth Scans [22] datasets. Experimental results show that our approach can effectively reduce the domain gap between the online 3D model repositories and the real depth scans with background noise. Our approach is significantly better than without domain adaptation and is superior to general-purpose domain adaptation techniques such as ADDA [34]. We provide an ablation study to justify the design choice of each component of our approach, including the unsupervised loss terms and the optimization strategy. Code is publicly available at <https://github.com/xingyizhou/3DKeypoints-DA>.

2. Related Works

Keypoint Detection. Keypoint detection from a single RGB or RGB-D image is a fundamental task in computer vision. We refer to [19, 44, 24, 8] for some recent advances on this topic. While most techniques focus on developing novel neural network architectures for this task, fewer works focus on addressing the issue of domain shifts between the training data and testing data, e.g., the setting described in this paper. In [44], the authors introduce a domain adaptation technique for 3D human pose estimation in the wild. Additionally for human pose estimation, [8] proposes to align the source and target label distributions using a GAN loss. We opt to use an alternate metric that offers more flexibility in addressing domain shifts. Similarly to our method, [24] also leverages the consistency across multiple views to boost the supervision on the target domain. However, the output of this approach is computed directly from the initial predictions from the source domain. In contrast, our approach only uses the initial predictions to initialize final predictions. Moreover, we utilize a latent configuration for synchronizing the predictions from multiple views, which avoids performing pair-wise analysis.

Multi-view supervision. RGB and RGB-D video sequences essentially consist of different views of the same underlying 3D environment. In the literature, people have utilized such weak supervision for various tasks such as 3D reconstruction, novel view synthesis and 2D keypoint prediction, e.g., [33, 39, 42, 15, 24]. Our work differs from most works in the sense that we do not assume that relative poses between cameras are known. Instead, we introduce a pose invariant metric to compare keypoint configurations.

Supervision from Big 3D Data. Thanks the availability of annotated big 3D data such as ModelNet [37] and ShapeNet [3], people have leveraged synthetic data generated from 3D models for various tasks, including image classification [37], object recognition [25, 21, 26], semantic segmentation [41], object reconstruction [27, 5, 31], pose

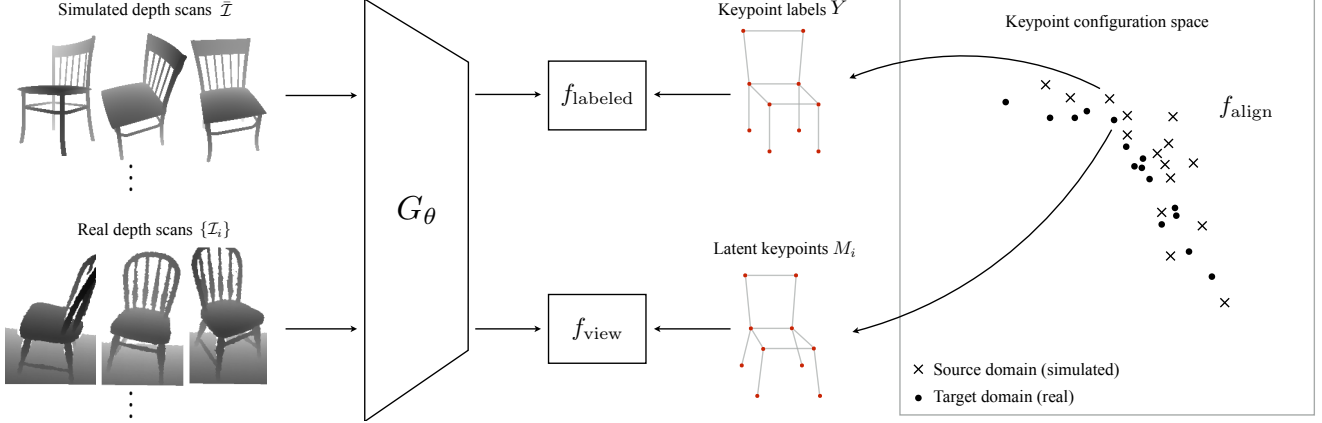


Figure 2: **Approach overview.** We train an end-to-end 3D keypoint prediction network G_θ from labeled simulated depth scans $\tilde{\mathcal{I}}$ of 3D models and unlabeled and unaligned real depth scans $\{\mathcal{I}_i\}$ of real world objects. We define three loss terms for training: the supervised labeled term f_{labeled} enforces prediction accuracy in the source domain where labels are available; the unsupervised view-consistency term f_{view} ensures keypoint predictions from different views are consistent in the target domain; the geometric alignment term f_{align} aligns the distribution of the predicted keypoints in the target domain with the source domain. See Section 4 for details.

estimation [28] and novel-view synthesis [29, 43]. The fundamental challenge of these approaches is that there are domain shifts between synthetic data and real RGB or RGB-D images. Most existing works focus on improving the simulation process to close this gap. In contrast, we focus on developing an unsupervised loss for domain adaptation.

Domain adaptation. Domain adaptation for various visual recognition tasks is an active research area in computer vision, and our problem falls into the general category of domain adaptation. It is beyond the scope of this paper to provide a comprehensive review of the literature, however we refer to [20, 9, 40, 10, 18, 38, 2, 13, 16, 35, 23] for recent advances and to [7] for a recent survey on this topic. A common strategy for unsupervised domain adaptation is to align the output distributions between source and target domains, e.g., either through explicit domain-wise maps or through use of a GAN. In contrast, our regularizations are tailored for the particular problem we consider, i.e., view-consistency and domain shifts caused by varying densities.

3. Problem Statement

We study the problem of predicting complete 3D keypoints of an underlying object from a single image or depth scan. We assume the input consists of a labeled dataset $\tilde{\mathcal{I}}$ and an unlabeled dataset \mathcal{I} . Moreover, the unlabeled dataset is comprised of N subsets $\mathcal{I}_i, 1 \leq i \leq N$, where each subset collects depth scans/images of the same object from different views. Such data naturally arises from RGB-D or RGB video sequences.

Each instance $I \in \tilde{\mathcal{I}}$ in the labeled dataset possesses a ground-truth label $Y(I) \in \mathbb{R}^{3 \times d}$, which is a matrix that col-

lects the coordinates of the ordered keypoints in its columns. Without losing generality, we assume that the 3D local coordinate system of I is chosen so that the centroid of $Y(I)$ is at the origin, i.e.,

$$Y(I)\mathbf{1} = 0. \quad (1)$$

It is expected that the source domain of the labeled dataset and the target domain of the unlabeled dataset are different (e.g., the source domain consists of synthetic images/scans and the target domain consists of real images/scans). Our goal is to train a neural network $G_\theta : \mathbb{R}^{m \times n} \rightarrow \mathbb{R}^{3 \times d}$ that takes an image from the target domain as input and outputs the predicted keypoints by leveraging both the labeled dataset $\tilde{\mathcal{I}}$ and unlabeled subsets $\mathcal{I}_i, 1 \leq i \leq N$. We call this problem unsupervised domain adaptation for 3D keypoint prediction.

Note that we do not assume the underlying cameras of each unlabeled subset are calibrated, or in other words, the relative transformations between different views of the same object are not required. Although it is possible to align the depth scans to obtain relative transformations, we found that such alignments are not always reliable in the presence of scanning discontinuities where little overlaps between consecutive scans are available. In contrast, our formulation treats relative camera poses as latent variables, which are optimized together with the network parameters.

4. Approach

In this section, we describe our detailed approach to unsupervised domain adaptation for 3D keypoint prediction. We first introduce a pose-invariant distance metric to compare keypoint configurations in Section 4.1. This allows us

to compare the predictions in different views without knowing the relative transformations between the views for uncalibrated datasets. We then present the formulation of our approach in Section 4.2. Finally, we discuss our optimization strategy in Section 4.3.

4.1. Pose-Invariant Distance Metric

The pose-invariant distance metric compares two keypoint configurations $X, Y \in \mathbb{R}^{3 \times d}$ described in different coordinate systems. Since the mean of each keypoint configuration is zero, we introduce a latent rotation R to account for the underlying relative transformation:

$$r(X, Y) = \min_{R \in SO(3)} \|RX - Y\|_{\mathcal{F}}^2, \quad (2)$$

where $\|\cdot\|_{\mathcal{F}}$ denotes the matrix Frobenius Norm. It is clear that $r(X, Y)$ is independent of the coordinate systems associated with X and Y , making it particularly suitable for comparing predictions from uncalibrated views and aligning the source domain and the target domain.

In the following, we discuss a few key properties of $r(X, Y)$ that will be used extensively in our approach. First of all, both $r(X, Y)$ and the gradient of $r(X, Y)$ with respect to each of its argument admit closed-form expressions. These are summarized in the following two propositions.

Proposition 1. $r(X, Y)$ admits the following analytic expression:

$$r(X, Y) = \|X\|_{\mathcal{F}}^2 + \|Y\|_{\mathcal{F}}^2 - 2 \cdot \text{trace}(R \cdot (XY^T))$$

where R is derived from the singular value decomposition (or SVD) of $YX^T = U\Sigma V^T$:

$$R = U \text{diag}(1, 1, s) V^T, \quad s = \text{sign}(\det(XY^T)). \quad (3)$$

Proof: See [14]. \square

Proposition 2. The gradient of $r(X, Y)$ with respect to X is given by

$$\frac{\partial r}{\partial X}(X, Y) = 2(X - R^T Y),$$

where R is given by Eq. (3).

Proof: Please refer to the supplemental material. \square

Our optimization procedure also frequently involves the following optimization problem that computes the weighted average X^* of a set of keypoint configurations $Y_i, 1 \leq i \leq n$ in the quotient space $\mathbb{R}^{3 \times d}/SO(3)$:

$$\begin{aligned} X^* &= \underset{X \in \mathbb{R}^{3 \times d}}{\text{argmin}} \sum_{i=1}^n c_i r(X, Y_i) \\ &= \underset{X \in \mathbb{R}^{3 \times d}}{\text{argmin}} \sum_{i=1}^n c_i \min_{R_i \in SO(3)} \|X - R_i^T Y_i\|_{\mathcal{F}}^2, \end{aligned} \quad (4)$$

where $c_i, 1 \leq i \leq n$ are constants. Although Eq. (4) does not admit a closed-form solution, it can be easily optimized via alternating minimization. Specifically, when X is fixed, each R_i can be computed independently using Proposition 1. When the R_i latent variables are fixed, X is simply given by the mean of $R_i^T Y_i$, i.e., $X = \frac{1}{\sum_{i=1}^n c_i} \sum_{i=1}^n c_i R_i^T Y_i$.

To make the solution unique, we always set $R_1 = I_3$. As shown in [1], such alternating minimization scheme admits a geometric convergence rate. Denoting X^k as the solution at iteration k , we stop the alternating minimization when $\|X^{k+1} - X^k\|_{\mathcal{F}} \leq 10^{-3}$. In our implementation, we found 8 – 10 iterations sufficient for convergence.

4.2. Formulation

To train the keypoint prediction network $G_{\theta}(\cdot)$, we introduce three loss terms, namely, a labeled term f_{labeled} , a view-consistency term f_{view} and a geometric alignment term f_{align} .

The labeled term f_{labeled} fits predictions on the source domain labeled dataset \mathcal{I} to the prescribed ground-truth labels. We use the regression loss under the L2-norm, which works well for 3D keypoint prediction tasks (c.f. [30, 44]):

$$f_{\text{labeled}} = \frac{1}{|\mathcal{I}|} \sum_{I \in \mathcal{I}} \|G_{\theta}(I) - Y(I)\|_{\mathcal{F}}^2. \quad (5)$$

The view-consistency term f_{view} is defined on the target domain to enforce consistency between the predictions from different views of the same object. In other words, there exist pairwise rotations that transform the predictions from one view to another. A straightforward approach is to minimize $r(G_{\theta}(I_{ij}), G_{\theta}(I_{ij'}))$, where I_{ij} and $I_{ij'}$ are different views of the same object. However, we found that such approach introduces a quadratic number of terms as the number of views increases and quickly becomes intractable. Therefore, we introduce a latent configuration $M_i \in \mathbb{R}^{3 \times d}$ for each unlabeled subset \mathcal{I}_i that characterizes the underlying ground-truth in the canonical frame. We then define the view consistency term as:

$$f_{\text{view}} = \frac{1}{N} \sum_{i=1}^N \frac{1}{|\mathcal{I}_i|} \sum_{I_{ij} \in \mathcal{I}_i} r(G_{\theta}(I_{ij}), M_i). \quad (6)$$

It is clear that minimizing f_{view} automatically aligns the predictions across different views. The key advantages of Eq. (6) over enforcing pairwise view-consistency are (i) the number of items is linear to the number of views, and (ii) as we will see immediately, the latent configurations $\{M_i\}$ allow us to easily formulate the geometric alignment term f_{align} .

The geometric alignment term f_{align} prioritizes that the latent configurations $\{M_i, 1 \leq i \leq N\}$, which characterize the predictions on the target domain, shall be consistent

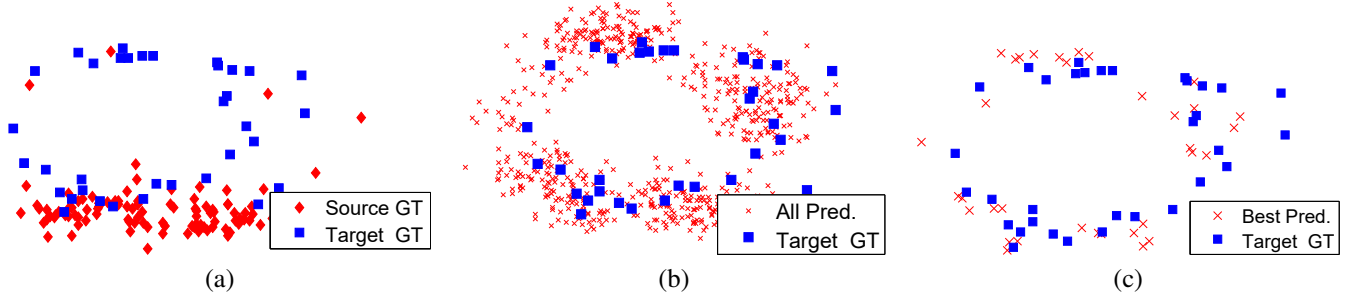


Figure 3: **Latent Distribution and View Selection.** This figure provides visualizations of label distributions and view selection for initializing the latent configurations from ModelNet (source domain) to Redwood (target domain) on the Chair category. All visualizations are done by 2D projections using the first two principal components. (a) Label distributions of the source and target domains. We can see there is a clear shift label distribution, but each instance in one domain is surrounded by instances from the other domain. (b) Visualizations of all predictions from different views. (c) Visualizations of the best prediction from each object.

with ground-truth labels $\{Y_I | I \in \bar{\mathcal{I}}\}$ of the source domain. This term is conceptually similar to the idea of aligning output distributions for unsupervised domain adaptation, but our formulation is tailored to the specific problem we consider in this paper. A straightforward formulation is to use the Earth-Mover Distance between $\{M_i, 1 \leq i \leq N\}$ and $\{Y(I) | I \in \bar{\mathcal{I}}\}$, which essentially aligns the two corresponding empirical distributions. However, we found that this strategy would force the alignment of keypoint configurations that are far apart, since the repetition counts of the same sub-types of an object may be different between the source and target domains (See Figure 3(a)). To address this issue, we propose to use the Chamfer distance for alignment:

$$f_{\text{align}} = \frac{1}{N} \sum_{i=1}^N \min_{I \in \bar{\mathcal{I}}} r(M_i, Y_I) + \frac{1}{|\bar{\mathcal{I}}|} \sum_{I \in \bar{\mathcal{I}}} \min_{1 \leq i \leq N} r(M_i, Y_I). \quad (7)$$

Intuitively, Eq. (7) still aligns the source and target domains, but it is insensitive to local density variations, and provides an effective way to address domain shifts.

We combine the labeled term f_{labeled} , the view-consistency term f_{view} and the geometric alignment term f_{align} into the final loss function:

$$\underset{\theta, \{M_i\}}{\text{minimize}} f_{\text{labeled}} + \lambda f_{\text{view}} + \mu f_{\text{align}}. \quad (8)$$

In our implementation, we set $\lambda = 1$ and $\mu = 0.1$.

4.3. Optimization

The major difficulty for optimizing Eq. (8) lies in the fact that the alignment term f_{align} is highly non-convex. In our experiments, we found that obtaining good initial values of the network parameters and latent variables is critical to achieving high-quality keypoint prediction network. In the following, we first introduce effective strategies to initial-

ize the variables. We then show how to refine the variables using alternating minimization.

Network Parameter Initialization. The network parameters are initialized by pre-training on the the source domain labeled dataset, i.e.,

$$\theta^{(0)} = \min_{\theta} \sum_{I \in \bar{\mathcal{I}}} \|G_{\theta}(I) - Y_I\|_{\mathcal{F}}^2. \quad (9)$$

It is then optimized via standard back-propagation.

Latent Configuration Initialization. We use the predictions obtained from the initial network $G_{\theta^{(0)}}(I_{ij}), I_{ij} \in \mathcal{I}_i$ to initialize each latent variable M_i . To this end, we define a score for each prediction and set M_i as the one with the highest score. The scoring function is motivated by the fact that the latent variables are expected to align with the source domain, we thus define an un-normalized density function:

$$p(M) = \sum_{I \in \bar{\mathcal{I}}} \exp\left(-\frac{r(M, Y(I))}{2\sigma^2}\right), \quad (10)$$

where σ is chosen as mean of $r(G_{\theta^{(0)}}(I_{ij}), Y(I))$ between the predicted configurations and their closest labeled instances. Given Eq. (10), we set

$$M_i^{(0)} = \underset{M \in \{G_{\theta^{(0)}}(I) | I \in \mathcal{I}_i\}}{\text{argmax}} p(M). \quad (11)$$

As illustrated in Figure 3(b-c), this strategy leads to initial configurations that are close to the underlying ground-truth.

Alternating Minimization. Given the initial network parameter $\theta^{(0)}$ and the initial latent configurations $M_i^{(0)}, 1 \leq i \leq N$, we then refine them by solving Eq. (8) via alternating minimization. With $M_i^{(k)}$ and $\theta^{(k)}$ we denote their values at iteration k . At each alternating minimization step, we first fix the latent variables to optimize the network pa-

rameters. This leads to computing

$$\begin{aligned} \theta^{(k+1)} = & \underset{\theta}{\operatorname{argmin}} \frac{1}{|\mathcal{I}|} \sum_{I \in \mathcal{I}} \|G_{\theta}(I) - Y_I\|_{\mathcal{F}}^2 \\ & + \frac{\lambda}{N} \sum_{i=1}^N \frac{1}{|\mathcal{I}_i|} \sum_{I \in \mathcal{I}_i} r(G_{\theta}(I), M_i^{(k)}). \end{aligned} \quad (12)$$

Utilizing Proposition 2, we apply stochastic gradient descent via back-propagation for solving Eq. (12).

We then fix the network parameters θ and optimize the latent variables $\{M_i^{(k+1)}\}$. In this case, Eq. (8) reduces to

$$\begin{aligned} \{M_i^{(k+1)}\} = & \underset{\{M_i\}}{\operatorname{argmin}} \frac{\mu}{|\mathcal{I}|} \sum_{I \in \mathcal{I}} \min_{1 \leq i \leq N} r(M_i, Y_I) \\ & + \frac{1}{N} \sum_{i=1}^N \left(\frac{\lambda}{|\mathcal{I}_i|} \sum_{I \in \mathcal{I}_i} r(G_{\theta^{(k)}}(I), M_i) + \mu \min_{I \in \mathcal{I}} r(M_i, Y_I) \right). \end{aligned} \quad (13)$$

We again apply alternating minimization to solve Eq. (13). In particular, we fix the closest point pairs given $\{M_i^{(k)}\}$:

$$\hat{I}(i) = \underset{I \in \mathcal{I}}{\operatorname{argmin}} r(M_i^{(k)}, Y_I), \quad \hat{i}(I) = \underset{1 \leq i \leq N}{\operatorname{argmin}} r(M_i^{(k)}, Y_I). \quad (14)$$

Given these closest pairs, we can optimize the latent configurations M_i independently via:

$$\begin{aligned} M_i^{(k+1)} = & \underset{M_i}{\operatorname{argmin}} \frac{\mu}{|\mathcal{I}|} \sum_{I | \hat{i}(I)=i} r(M_i, Y_I) \\ & + \frac{1}{N} \left(\frac{\lambda}{|\mathcal{I}_i|} \sum_{I \in \mathcal{I}_i} r(G_{\theta^{(k)}}(I), M_i) + \mu r(M_i, Y_{\hat{I}(i)}) \right). \end{aligned} \quad (15)$$

Eq. (15) admits a form of Eq. (4), and we apply the procedure described above to solve Eq. (15). In our experiments, we typically apply the inner alternating minimizations each 5 epochs for training the network parameters θ .

5. Evaluation

In this section, we evaluate the proposed unsupervised domain adaptation method for 3D keypoint prediction. We first describe the experimental setup in Section 5.1. We then present qualitative and quantitative results and compare our technique to baseline approaches in Section 5.2. Finally, we present an ablation study to evaluate each component of our approach in Section 5.3 and extend our method to RGB images in Section 5.4.

5.1. Experimental Setup

Dataset. The focus of our evaluation is on the chair object class because of its presence across many 3D model and depth scan datasets. Rendered depth scans of chairs from

Target	#Train Models	#Test Models	Avg #frames
ModelNet[37]	899	100	Inf
ShapeNet [3]	2500	100	Inf
Redwood [4]	200	35	150
3DCNN [22]	9	3	80

Table 1: **Statistics of the datasets.** We show the number of models and the average number of frames per model.

the synthesized ModelNet [37] dataset serve as our source domain, and we test our domain adaptation method on three different target domains, namely another synthesized 3D model dataset ShapeNet [3], real depth scans from the Redwood Object Scans dataset [4], real depth scans from the 3DCNN dataset [22]. To provide keypoint labels for our source domain, we manually annotate the training samples in ModelNet with Meshlab [6]. To evaluate the accuracy of our system, we also annotate chair keypoints on our target domain datasets. This annotation is done by recovering the object’s 3D mesh and each frame’s camera pose from a depth video sequence. By knowing each frame’s camera pose in relation to the reconstructed mesh, we can propagate the keypoint annotation to the whole sequence. We keep the frames which all the 2D projection of keypoints are within the image and keep the models with at least 20 different frames. A summary of the number of samples of the four datasets used in our experiments is presented in Table 1. As a natural extension, we also test our method on the RGB images from the same Redwood dataset [4].

Data pre-processing. We assume the camera intrinsic and object’s 3D bounding box are known both in training and testing depth images. We use the 2D projection of the 3D bounding box to crop the image. Additionally, the input depth images are centered by the mean depth and the depth values are normalized by the diagonal length of the 3D bounding box. Aside from the images, all keypoints are converted and evaluated in a unified coordinate system. Given a configuration, we subtract their mean and normalize by the diagonal length of the 3D bounding box.

Evaluation protocol. Similar to [36], we measure the Average distance Error (AE) between each predicted keypoint configuration and the corresponding annotation and plot the Percentage of Correct Keypoint (PCK) with respect to a threshold for each method for detailed comparison. We also introduce a new metric, Pose-invariant Average distance Error (PAE) expressed in Equation 2, for a better illustration of how our proposed method works. The AE and PAE are show in percentage since they respect to the relative ratio to the diagonal length of the 3D bounding box.

Baseline methods. We consider three baseline methods for experimental evaluation.

Target-Metric	Default-AE	ADDA-AE	Ours-AE	Supervised-AE	Default-PAE	ADDA-PAE	Ours-PAE	Supervised-PAE
ModelNet [37]	-	-	-	5.56	-	-	-	4.76
ShapeNet [3]	6.97	6.98	6.60	5.82	5.77	5.89	5.32	4.77
RedwoodDepth [4]	16.01	15.44	12.76	8.67	10.73	10.13	8.27	5.68
3DCNN [22]	11.61	11.81	10.60	6.73	8.15	8.19	7.25	4.98
RedwoodRGB [4]	27.59	26.16	25.24	11.90	13.44	12.31	11.38	7.67

Table 2: Results of our proposed methods before and after domain adaptation on different target domains. We show Average distance Error (AE) and Pose-Invariant Average distance Error (PAE) in percentage, the lower the better.

- **Baseline I.** We first test performance without any domain adaptation techniques, namely we directly apply the keypoint predictor trained on the source domain to the target domain. This baseline serves as a performance lower bound for accessing domain adaptation techniques.
- **Baseline II.** We implement a state-of-the-art deep unsupervised domain adaptation technique described in [34], which encourages domain confusion by fine-tuning the feature extractor on the target domain.
- **Baseline III.** We apply supervised keypoint prediction on the target domain. To this end, we annotate 50 additional models from each domain and fine-tune Baseline I on these labeled instances. This baseline serves as a performance upper bound for accessing domain adaptation techniques.

Besides these baseline approaches, we also conduct an ablation study to evaluate each component of our approach.

Implementation details. We use ResNet50 [12] pre-trained on ImageNet as our keypoint prediction network G_θ . In order to fit our depth scans to the ResNet50 input (and additionally, to allow for natural extension to the RGB image domain), we duplicate the depth channel three times. The network is first trained on source domain $\bar{\mathcal{I}}$ for 120 epochs, and then fine-tuned on a specific target domain \mathcal{I} for 30 epochs. The network is trained using a SGD optimizer via back-propagation, with learning rate 0.01 (dropped to 0.001 after 20 epochs), batch size 64, momentum 0.9 and weight decay $1e-4$, which are all the default parameters in Resnet50 [12]. Our implementation is done in the PyTorch.

5.2. Analysis of Results

Table 2, Table 3, and Figure 5 present the quantitative and qualitative results of our approach.

Qualitative results. As illustrated in Figure 5, our approach yields keypoint structures that are consistent with the underlying ground-truths. Even under significant background noise and incomplete observations, our approach leads to faithful structures. Exceptions include the case for chair

types that involve swivel bases. In this case, the predicted legs may be tilted. This is expected since the annotations may become unreliable in cases when the legs do not fall directly below the seat corners.

Quantitative assessment. As shown in Table 2, the mean deviation of our approach in the two real depth scan datasets Redwood [4] and 3DCNN [22] are 12.76% and 10.60% of the diagonal length of object bounding box, respectively. This translates to approximately 7-10 cm, which is fairly accurate when compared to the radius of a chair’s base.

Analyses of performance across different datasets. Our method gives consistent performance improvements on all three target depth domains. For the synthesized dataset ShapeNet [3], which has a relatively small domain shift from the supervised training set, our unsupervised terms are still able to push error rates close to the supervised upper bound. The advantages of our proposed method can be best observed in the Redwood dataset [4], where using our full error terms leads to a 44% step towards the supervised performance upper-bound. Additionally, the improvement in 3DCNN Dataset [22] is still decent despite the very limited available models and poor depth image quality.

Analysis of performance gain. Our performance gains can be attributed to our network learning more plausible keypoint configuration shapes, which is supported by the fact that the improvement of AE is always close to that of PAE. This is expected because our unsupervised terms are viewpoint-invariant and focus on improving the keypoint configuration shape.

Comparison to ADDA [34]. Our approach is superior to the state-of-the-art unsupervised domain adaptation technique [34] in the keypoint estimation task, which aligns the feature distributions of the source and target domains. It is complementary to our approach that constraints on the label space. We argue that there are more structure to rely on in label space for rigid objects. Another important factor is that view consistency is not Incorporated in ADDA [34]. Quantitatively, ADDA does not give consistent performance boost based on our implementation. Its AE in Redwood dataset is 15.44% while ours is 12.76%.

f Target domain	ShapeNet(%)	Redwood depth(%)
Ours	6.60	12.76
Re-initialize	6.66	13.43
Drop view	6.70	13.95
Drop align	6.67	12.97

Table 3: **Ablation study on ShapeNet and Redwood Object Scans dataset.** We show the Average distance Error (AE) in percentage for each approach.

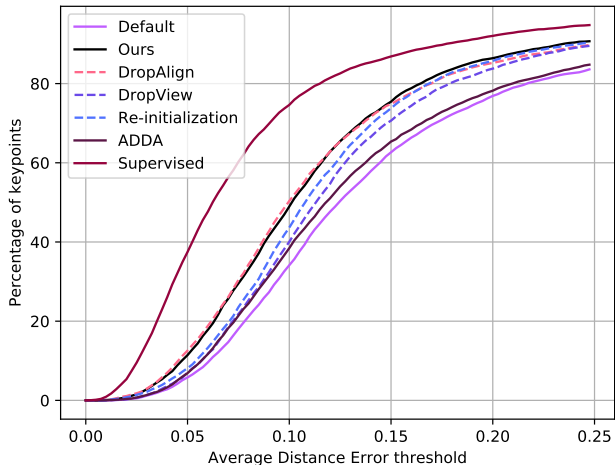


Figure 4: **Baseline & Ablation Study.** Comparisons between our approach with alternative approaches on Redwood depth Dataset [4]. The Figure shows Percentage of Correct Keypoints (PCK) under a threshold.

5.3. Ablation Study

We present ablation studies to justify each component of our approach. Due to space constraints, we restrict our study to the representative target domains, Redwood depth and ShapeNet.

Dropping the view-consistency term. We test the effects of dropping the view-consistency term. In this case, we simply align the output from all the depth scans with annotations of the source domain. As shown in Table 3 and Figure 4, the performance drops considerably compared to our full term, while is still better than without adaptation.

Dropping the alignment term. Merely utilizing the view consistency term can significantly reduce the testing error. It can be interpreted as the network updating the latent variables in a self-guided manner, based on the consistency between different views. If the predictions on the majority of views are consistent with one another, the keypoint configuration obtained by averaging all the predictions can serve as a reliable guidance to correct the bad outliers.

Latent configuration updates versus re-initialization Instead of updating the latent configurations M_i by solving

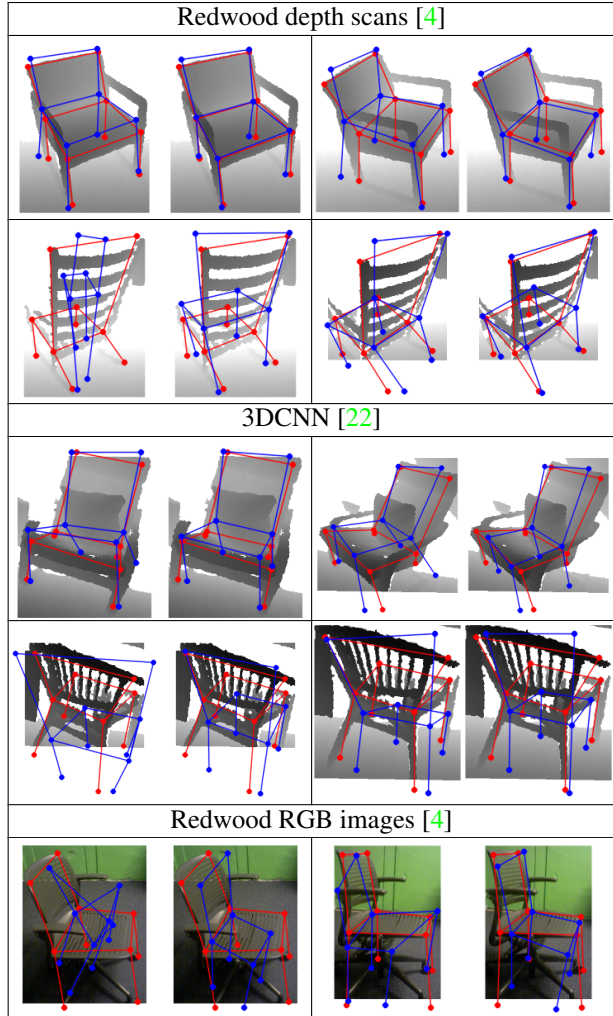


Figure 5: **Qualitative results.** We compare 3D keypoint predictions (blue) before (left) and after (right) our unsupervised domain adaptation on different datasets. For each model we show 2 views. Reference ground-truth are in red.

Eq. 15, we can apply Eq. 11 to re-initialize the latent configurations, which is also consistent with our training framework. The results is worse than updating M_i by minimizing the view-consistency term, showing an advantage of our alternating minimization schema.

5.4. Extension to RGB images

Our framework can seamlessly be applied in domain adaptation to RGB images. We show our preliminary results on Tab. 2, and it is evident that our proposed method is able to reduce the AE from the baseline without domain adaptation. As shown in Fig. 5, our method helps regularize the output when the before-adaptation baseline predicts a seemingly random point set.

6. Conclusions and Future Work

In this paper, we introduced an unsupervised domain adaptation approach for keypoint prediction from a single depth image. Our approach combines two task-specific regularizations, i.e., view-consistency and label distributions alignment of the source and target domains. Experimental results show that our approach is significantly better than without domain adaptation and is superior to state-of-the-art generic domain adaptation methods.

References

- [1] J. C. Bezdek and R. J. Hathaway. Convergence of alternating optimization. *Neural, Parallel Sci. Comput.*, 11(4):351–368, Dec. 2003. 4
- [2] K. Bousmalis, N. Silberman, D. Dohan, D. Erhan, and D. Krishnan. Unsupervised pixel-level domain adaptation with generative adversarial networks. In *The IEEE Conference on Computer Vision and Pattern Recognition (CVPR)*, July 2017. 3
- [3] A. X. Chang, T. A. Funkhouser, L. J. Guibas, P. Hanrahan, Q. Huang, Z. Li, S. Savarese, M. Savva, S. Song, H. Su, J. Xiao, L. Yi, and F. Yu. Shapenet: An information-rich 3d model repository. *CoRR*, abs/1512.03012, 2015. 2, 6, 7
- [4] S. Choi, Q.-Y. Zhou, S. Miller, and V. Koltun. A large dataset of object scans. *arXiv:1602.02481*, 2016. 1, 2, 6, 7, 8
- [5] C. B. Choy, D. Xu, J. Gwak, K. Chen, and S. Savarese. 3d-r2n2: A unified approach for single and multi-view 3d object reconstruction. In *Proceedings of the European Conference on Computer Vision (ECCV)*, 2016. 2
- [6] P. Cignoni, M. Callieri, M. Corsini, M. Dellepiane, F. Ganovelli, and G. Ranzuglia. Meshlab: an open-source mesh processing tool. In *Eurographics Italian Chapter Conference*, volume 2008, pages 129–136, 2008. 6
- [7] G. Csurka. Domain adaptation for visual applications: A comprehensive survey. *CoRR*, abs/1702.05374, 2017. 3
- [8] H.-Y. Fish Tung, A. W. Harley, W. Seto, and K. Fragkiadaki. Adversarial inverse graphics networks: Learning 2d-to-3d lifting and image-to-image translation from unpaired supervision. In *The IEEE International Conference on Computer Vision (ICCV)*, Oct 2017. 2
- [9] T. Gebru, J. Hoffman, and L. Fei-Fei. Fine-grained recognition in the wild: A multi-task domain adaptation approach. In *The IEEE International Conference on Computer Vision (ICCV)*, Oct 2017. 3
- [10] B. Gholami, O. (Oggi) Rudovic, and V. Pavlovic. Punda: Probabilistic unsupervised domain adaptation for knowledge transfer across visual categories. In *The IEEE International Conference on Computer Vision (ICCV)*, Oct 2017. 3
- [11] S. Gupta, P. A. Arbeláez, R. B. Girshick, and J. Malik. Aligning 3D models to RGB-D images of cluttered scenes. In *Computer Vision and Pattern Recognition (CVPR)*, 2015. 1
- [12] K. He, X. Zhang, S. Ren, and J. Sun. Deep residual learning for image recognition. In *Proceedings of the IEEE conference on computer vision and pattern recognition*, pages 770–778, 2016. 7
- [13] S. Herath, M. Harandi, and F. Porikli. Learning an invariant hilbert space for domain adaptation. In *The IEEE Conference on Computer Vision and Pattern Recognition (CVPR)*, July 2017. 3
- [14] B. K. P. Horn. Closed-form solution of absolute orientation using unit quaternions. *Journal of the Optical Society of America A*, 4(4):629–642, 1987. 4
- [15] E. Kalogerakis, M. Averkiou, S. Maji, and S. Chaudhuri. 3d shape segmentation with projective convolutional networks. *CoRR*, abs/1612.02808, 2016. 2
- [16] P. Koniusz, Y. Tas, and F. Porikli. Domain adaptation by mixture of alignments of second- or higher-order scatter tensors. In *The IEEE Conference on Computer Vision and Pattern Recognition (CVPR)*, July 2017. 3
- [17] Y. Li, A. Dai, L. Guibas, and M. Nießner. Database-assisted object retrieval for real-time 3d reconstruction. In *Computer Graphics Forum*, volume 34. Wiley Online Library, 2015. 1
- [18] F. Maria Carlucci, L. Porzi, B. Caputo, E. Ricci, and S. Rota Bulò. Autodial: Automatic domain alignment layers. In *The IEEE International Conference on Computer Vision (ICCV)*, Oct 2017. 3
- [19] A. Newell, K. Yang, and J. Deng. Stacked hourglass networks for human pose estimation. In *ECCV (8)*, volume 9912 of *Lecture Notes in Computer Science*, pages 483–499. Springer, 2016. 2
- [20] P. Panareda Busto and J. Gall. Open set domain adaptation. In *The IEEE International Conference on Computer Vision (ICCV)*, Oct 2017. 3
- [21] X. Peng, B. Sun, K. Ali, and K. Saenko. Learning deep object detectors from 3d models. In *ICCV*, pages 1278–1286. IEEE Computer Society, 2015. 2
- [22] C. R. Qi, H. Su, M. Nießner, A. Dai, M. Yan, and L. J. Guibas. Volumetric and multi-view cnns for object classification on 3d data. In *Proceedings of the IEEE Conference on Computer Vision and Pattern Recognition*, pages 5648–5656, 2016. 2, 6, 7, 8
- [23] S. Sankaranarayanan, Y. Balaji, C. D. Castillo, and R. Chellappa. Generate to adapt: Aligning domains using generative adversarial networks. *CoRR*, abs/1704.01705, 2017. 3
- [24] T. Simon, H. Joo, I. Matthews, and Y. Sheikh. Hand keypoint detection in single images using multiview bootstrapping. In *The IEEE Conference on Computer Vision and Pattern Recognition (CVPR)*, July 2017. 2
- [25] S. Song and J. Xiao. Sliding shapes for 3d object detection in depth images. In *ECCV (6)*, volume 8694 of *Lecture Notes in Computer Science*, pages 634–651. Springer, 2014. 2
- [26] S. Song and J. Xiao. Deep Sliding Shapes for amodal 3D object detection in RGB-D images. 2016. 2
- [27] S. Song, F. Yu, A. Zeng, A. X. Chang, M. Savva, and T. Funkhouser. Semantic scene completion from a single depth image. *Proceedings of 30th IEEE Conference on Computer Vision and Pattern Recognition*, 2017. 2
- [28] H. Su, C. R. Qi, Y. Li, and L. J. Guibas. Render for cnn: Viewpoint estimation in images using cnns trained with rendered 3d model views. In *The IEEE International Conference on Computer Vision (ICCV)*, December 2015. 3

- [29] H. Su, F. Wang, E. Yi, and L. J. Guibas. 3d-assisted feature synthesis for novel views of an object. In *ICCV*, pages 2677–2685. IEEE Computer Society, 2015. 3
- [30] X. Sun, J. Shang, S. Liang, and Y. Wei. Compositional human pose regression. In *The IEEE International Conference on Computer Vision (ICCV)*, Oct 2017. 4
- [31] M. Tatarchenko, A. Dosovitskiy, and T. Brox. Multi-view 3d models from single images with a convolutional network. In *ECCV (7)*, volume 9911 of *Lecture Notes in Computer Science*, pages 322–337. Springer, 2016. 2
- [32] S. Tulsiani and J. Malik. Viewpoints and keypoints. *CoRR*, abs/1411.6067, 2014. 1
- [33] S. Tulsiani, T. Zhou, A. A. Efros, and J. Malik. Multi-view supervision for single-view reconstruction via differentiable ray consistency. *CoRR*, abs/1704.06254, 2017. 2
- [34] E. Tzeng, J. Hoffman, K. Saenko, and T. Darrell. Adversarial discriminative domain adaptation. *arXiv preprint arXiv:1702.05464*, 2017. 2, 7
- [35] E. Tzeng, J. Hoffman, K. Saenko, and T. Darrell. Adversarial discriminative domain adaptation. In *The IEEE Conference on Computer Vision and Pattern Recognition (CVPR)*, July 2017. 3
- [36] J. Wu, T. Xue, J. J. Lim, Y. Tian, J. B. Tenenbaum, A. Torralba, and W. T. Freeman. Single image 3d interpreter network. *CoRR*, abs/1604.08685, 2016. 6
- [37] Z. Wu, S. Song, A. Khosla, F. Yu, L. Zhang, X. Tang, and J. Xiao. 3d shapenets: A deep representation for volumetric shapes. In *CVPR*, pages 1912–1920, 2015. 2, 6, 7
- [38] H. Yan, Y. Ding, P. Li, Q. Wang, Y. Xu, and W. Zuo. Mind the class weight bias: Weighted maximum mean discrepancy for unsupervised domain adaptation. In *The IEEE Conference on Computer Vision and Pattern Recognition (CVPR)*, July 2017. 3
- [39] X. Yan, J. Yang, E. Yumer, Y. Guo, and H. Lee. Perspective transformer nets: Learning single-view 3d object reconstruction without 3d supervision. *CoRR*, abs/1612.00814, 2016. 2
- [40] Y. Zhang, P. David, and B. Gong. Curriculum domain adaptation for semantic segmentation of urban scenes. In *The IEEE International Conference on Computer Vision (ICCV)*, Oct 2017. 3
- [41] Y. Zhang, S. Song, E. Yumer, M. Savva, J.-Y. Lee, H. Jin, and T. Funkhouser. Physically-based rendering for indoor scene understanding using convolutional neural networks. *The IEEE Conference on Computer Vision and Pattern Recognition (CVPR)*, 2017. 2
- [42] B. Zhao, X. Wu, Z. Cheng, H. Liu, and J. Feng. Multi-view image generation from a single-view. *CoRR*, abs/1704.04886, 2017. 2
- [43] T. Zhou, S. Tulsiani, W. Sun, J. Malik, and A. A. Efros. View synthesis by appearance flow. In *ECCV*, 2016. 3
- [44] X. Zhou, Q. Huang, X. Sun, X. Xue, and Y. Wei. Towards 3d human pose estimation in the wild: A weakly-supervised approach. In *The IEEE International Conference on Computer Vision (ICCV)*, Oct 2017. 2, 4